INSTITUTE OF PHYSICS PUBLISHING PHYSICS IN MEDICINE AND BIOLOGY

Phys. Med. Biol. **49** (2004) 4745–4756 PII: S0031-9155(04)83132-4

Photoacoustic determination of blood vessel diameter

Roy G M Kolkman[1], John H G M Klaessens[2], Erwin Hondebrink[1], Jeroen C W Hopman[2], Frits F M de Mul[1], Wiendelt Steenbergen[1], Johan M Thijssen[2] and Ton G van Leeuwen[1]

[1] Biophysical Engineering, Faculty of Science and Technology, University of Twente, PO Box 217, 7500 AE Enschede, The Netherlands
[2] Clinical Physics laboratory, Department of Paediatrics, University Medical Center Nijmegen, PO Box 9109, 6500 HB Nijmegen, The Netherlands

E-mail: r.g.m.kolkman@utwente.nl

Received 5 July 2004
Published 24 September 2004
Online at stacks.iop.org/PMB/49/4745
doi:10.1088/0031-9155/49/20/006

Abstract

A double-ring sensor was applied in photoacoustic tomographic imaging of artificial blood vessels as well as blood vessels in a rabbit ear. The peak-to-peak time (τ_{pp}) of the laser (1064 nm) induced pressure transient was used to estimate the axial vessel diameter. Comparison with the actual vessel diameter showed that the diameter could be approximated by $2c\tau_{pp}$, with c the speed of sound in blood. Using this relation, the lateral diameter could also precisely be determined. *In vivo* imaging and monitoring of changes in vessel diameters was feasible. Finally, acoustic time traces were recorded while flushing a vessel in the rabbit ear with saline, which proved that the main contribution to the laser-induced pressure transient is caused by blood inside the vessel and that the vessel wall gives only a minor contribution.

1. Introduction

In recent years, there has been a wide interest in developing new techniques for non-invasive imaging of blood vessels and blood containing structures in tissue, such as tumours. Photoacoustic imaging (PAI), also called optoacoustic imaging, is an ideal candidate because this hybrid technique is based on the generation of acoustic waves by pulsed light being absorbed by tissue chromophores such as haemoglobin in blood (Kolkman *et al* 2003, Kruger *et al* 2003, Niederhauser *et al* 2003, Oraevsky *et al* 2001, Viator *et al* 2003, Wang *et al* 2003). The induced temperature rise generates a thermoelastic pressure transient, whose amplitude is dependent on the amount of absorbed light, being determined by the local energy fluence (J m^{-2}) and the optical absorption coefficient of the target. Measurement of this pressure transient using piezoelectric sensors is the most commonly used method in photoacoustic

imaging, although optical methods for detection of acoustic waves have been developed as well (Beard *et al* 2000, Niederhauser *et al* 2002, Paltauf *et al* 1999, Payne *et al* 2003). From the time of flight of this pressure wave to reach the tissue surface (detector position), the position of the photoacoustic source can be calculated when the speed of sound in tissue is known.

The advantage of PAI over purely optical techniques, such as diffuse optical tomography, is that the image resolution is not limited by the large amount of scattering of light by tissue. The resolution that can be achieved is solely determined by instrumental properties, such as the laser pulse duration, the geometry and bandwidth of the ultrasound-detection system, and the image reconstruction algorithm. The resulting image of the absorber distribution can be used for the quantification of blood vessel size or the vessel density, which is not only important for screening of tissue, but also for monitoring of treatment effects. Therefore, in this paper the feasibility of photoacoustic imaging to determine the vessel diameter is investigated. Results are presented from experiments on artificial blood vessels with various sizes. In addition the diameter of an artery *in vivo* in a rabbit ear was monitored.

2. Materials and methods

2.1. Lowering hematocrit

To investigate the effect of the absorption coefficient and/or hematocrit on our results, the hematocrit of the blood was lowered by adding phosphate-buffered saline (PBS) to the blood. The hematocrit was determined by centrifuging a sample of the diluted suspensions in a hematocrit tube for 10 min at 2500 rpm and measuring the ratio between the packed cell length and the total length with a ruler. A correction was made for 4% of trapped plasma by multiplying the ratio with 0.96.

2.2. Photoacoustic imaging

To perform PAI, light pulses were guided to the sample by a glass fibre (ø 600 μm, NA = 0.22) that was integrated in a home-built double-ring photoacoustic sensor, which has been extensively described elsewhere (Kolkman *et al* 2003, 2004). In short, this double-ring sensor consisted of two concentric ring-shaped electrodes with equal areas. The pressure transients were detected by 25 μm thick PVdF, biaxially stretched, electrically polarized, with one side metallized Au/Pt (Piezotech SA, France), which was glued to the electrodes. This sensor had an angular aperture of 1.5° (–6 dB of directivity pattern) for acoustic signals with a peak-to-peak time of 67 ns. The time traces detected by this sensor were digitized and the acquisition was synchronised on the Q-switch trigger generated by the laser. As the sensor had a narrow angular aperture, the measured time traces could be regarded as one-dimensional depth images (amplitude (A)-scans) of photoacoustic sources inside the measurement volume. The sensor was mounted on a translation stage to enable scanning which allowed us to obtain a 2D dataset (scan direction versus depth) of PA signals. To reduce lateral broadening (in the scan direction) of the vessels in the image, the zero-time-shift cross correlation value of the two signals of the separate ring-shaped electrodes was used as a weight factor in the image. This procedure was described in more detail elsewhere (Kolkman *et al* 2004).

2.3. Signal and image processing

To obtain quantitative information on the dimensions of the absorber, the measured pressure transients were further analysed using the models by Sigrist and Kneubühl (1978) and

Hoelen and de Mul (1999). In these models the photoacoustic source is a spherical source with a Gaussian absorption distribution $A(z)$, as a function of depth z, which is described by

$$A(z) \propto \exp\left[-\frac{1}{2}\left(\frac{z-r}{R_\sigma}\right)^2\right], \tag{1}$$

with R_σ the $1/\sqrt{e}$ radius of this Gaussian absorption distribution and r the distance from source to detector. The bipolar pressure transient that is generated by this source, is characterized by its peak-to-peak time τ_{pp} (time difference between the occurrence of the positive and negative peak), the zero-crossing time $\tau = r/\,c$, with c the speed of sound, and amplitude $P_{\max}$:

$$P(\mathbf{r}, t) = -P_{\max}(\mathbf{r})\sqrt{e}\frac{t-\tau}{1/2\tau_{pp}}\exp\left[-\frac{1}{2}\left(\frac{t-\tau}{\frac{1}{2}\tau_{pp}}\right)^2\right] \tag{2}$$

with τ_{pp} being expressed as

$$\tau_{pp} = \sqrt{\left(\frac{2R_\sigma}{c}\right)^2 + 2\tau_l^2} \tag{3}$$

with τ_l half the pulse duration between the $1/\sqrt{e}$ points of the temporal profile of the laser pulse.

To visualize the cross-section of the vessels in a 2D image (scan direction versus depth), equation (2) was fitted to the measured time traces (A-scans), with $P_{\max}$, τ_{pp} and τ as free running parameters. The resulting fit was integrated over time (i.e. depth) to obtain a representation of the absorption distribution $A(z)$:

$$A(z) \propto \exp\left[-\frac{1}{2}\left(\frac{z-c\tau}{\frac{1}{2}c\tau_{pp}}\right)^2\right]. \tag{4}$$

By plotting these absorption distributions next to each other, a 2D image of the absorbing structure was obtained.

The (fitted) peak-to-peak time contains information about the axial size of the source, which in theory is spherical. Here, as a first approximation, we will extend this model to cylindrical sources with diameter ϕ (m) using a dimensionless scaling factor a, which will be determined by our experimental data. Then equation (3) becomes

$$\tau_{pp} = \sqrt{\left(\frac{\phi}{ac}\right)^2 + 2\tau_l^2}. \tag{5}$$

In the case of small vessels, with $\phi/(ac)$ much smaller than the laser pulse duration, the peak-to-peak time will be mainly determined by the laser pulse duration.

Substituting equation (5) into equation (4) and assuming that the laser-pulse duration is much shorter than the acoustic transit time through the diameter ϕ ($\tau_{pp} = \phi/(ac)$) results in

$$A(z) \propto \exp\left[-\frac{1}{2}\left(\frac{z-c\tau}{\phi/2a}\right)^2\right]. \tag{6}$$

For $z - c\tau = \pm\frac{1}{2}\phi$, $A(z)$ represents the axial diameter of the vessel which means that this diameter can be indicated in the 2D images by plotting the contour line corresponding to $\exp\left(-\frac{1}{2}\,a^2\right)$.

3. Experiments

3.1. In vitro experiments

Artificial blood vessels made of silicon rubber tubes with various diameters, filled with flowing human blood (anti-coagulated with Lithium heparin), were immersed in a 10% Intralipid-10% dilution with a reduced scattering coefficient of 0.75 mm^{-1} at a wavelength of 1064 nm (van Staveren *et al* 1991). The actual inner diameter of the artificial vessels, measured with a calibrated microscope, were 0.38, 0.58, 0.85, 1.05 and 1.25 $\pm$ 0.05 mm. The vessels were positioned at a depth of 6 mm with respect to the sensor and were illuminated by the fibre in the centre of the photoacoustic sensor. A pulse energy of 3 mJ was applied at a wavelength of 1064 nm, with a repetition rate of 500 Hz and a pulse duration of 8 ns (DiNY pQ, IB Laser AG, Berlin, Germany). The photoacoustic signals were digitized by a dual channel oscilloscope-card (NI PCI-5112, 100 Msample s^{-1}, 100 MHz bandwidth, National Instruments). A scan perpendicular to the vessel was made by 268 subsequent A-scans (no averaging), equidistantly positioned with 18.6 μm spacing. The total measurement time was in this case 0.5 s.

Next, the A-scans were analysed as described above to determine the axial vessel diameter. The lateral diameter of the vessel was estimated from the absorption distribution as visualized in the 2D images.

To investigate the effect of the hematocrit on our results, the axial diameter of the vessel was also determined for a hematocrit of 29%.

3.2. In vivo experiments

Experiments were performed on blood vessels in the ear of a rabbit to explore the feasibility of photoacoustics to estimate and monitor vessel diameter *in vivo*. The Ethical Committee on Animal Research of the University of Nijmegen approved the experiments described in this work. The rabbit (New Zealand white rabbit, $\sim$2 kg) was anaesthetized and, after orotracheal intubation, mechanically ventilated. The ear of the rabbit was shaved and placed on foam rubber. Acoustic coupling between the tissue surface and photoacoustic sensor was obtained by using an optical transparent ultrasound contact gel (Sonogel®, Bad Camberg, Germany).

Acoustic signals were generated by illuminating the ear with 1 mJ/pulse at a pulse repetition rate of 50 Hz, with a wavelength of 1064 nm and pulse duration of 15 ns (LS2139, Lotis TII). The radiant exposure at the ear was about 14 mJ cm^{-2} per pulse. The photoacoustic signals were digitized by a dual channel digital oscilloscope (TDS220—Tektronix, 1 Gsample s^{-1}, 100 MHz bandwidth) operating at a sample rate of 250 Msample s^{-1}.

A 2D set of A-scans of the auricular artery in the ear of the rabbit was obtained by 61 A-scans, equidistantly positioned with 0.1 mm spacing, along line 1 (figure 1), resulting in a total B-scan time of 2 min. A second scan was made near the bifurcation along line 2 (figure 1), consisting of 31 subsequent A-scans with a spacing of 0.1 mm.

After imaging these two vessels, the sensor was placed in one steady position above the centre of one of these vessels and the photoacoustic signals were measured continuously. Including the data transfer from the oscilloscope to the computer, the total acquisition time for one photoacoustic time trace, consisting of 16 averages, was about 1.3 s. To change the size of the vessel it was alternately occluded and released proximal to the measurement position (upstream) by application of external pressure. The axial vessel diameter was determined from the peak-to-peak time of the measured pressure transients as described in the preceding section.

To investigate the contribution of the vessel wall to the acoustic pressure transient, a vein was flushed with saline, replacing the blood for a few seconds. Flushing with saline was

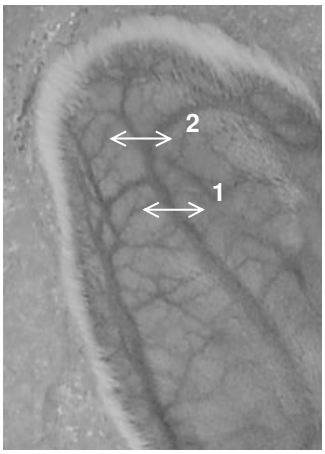

Figure 1. Photograph of the rabbit-ear with the blood vessel structure clearly visible. The arrows indicate the regions where a scan was made.

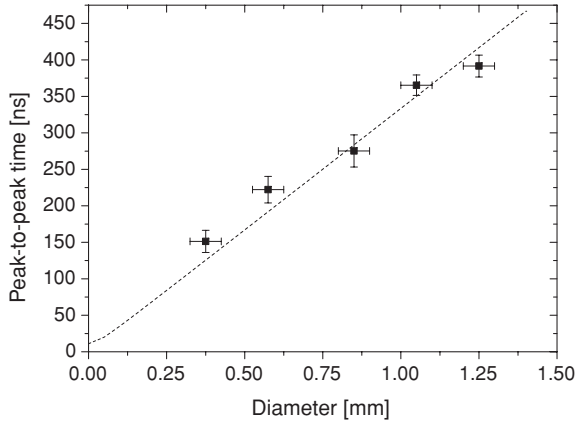

Figure 2. Peak-to-peak time of the pressure transients generated by artificial blood vessels with a diameter ranging from 0.38 to 1.25 $\pm$ 0.05 mm. Dashed line indicates the estimated relation between vessel diameter and peak-to-peak time (equation (5)).

carried out by injection of saline through a cannula positioned proximal to the measurement position, placed well outside the measurement site.

4. Results

4.1. In vitro experiments

The peak-to-peak time at the centre position of the artificial vessels was determined by fitting equation (2) to the measured pressure transient. The resulting peak-to-peak times, plotted as a function of vessel diameters (figure 2), were fitted to our model (equation (5)) and this yielded $a = 2.0 \pm 0.1$. Using our image-reconstruction approach, the absorption distribution could be reconstructed for all the five artificial blood vessels

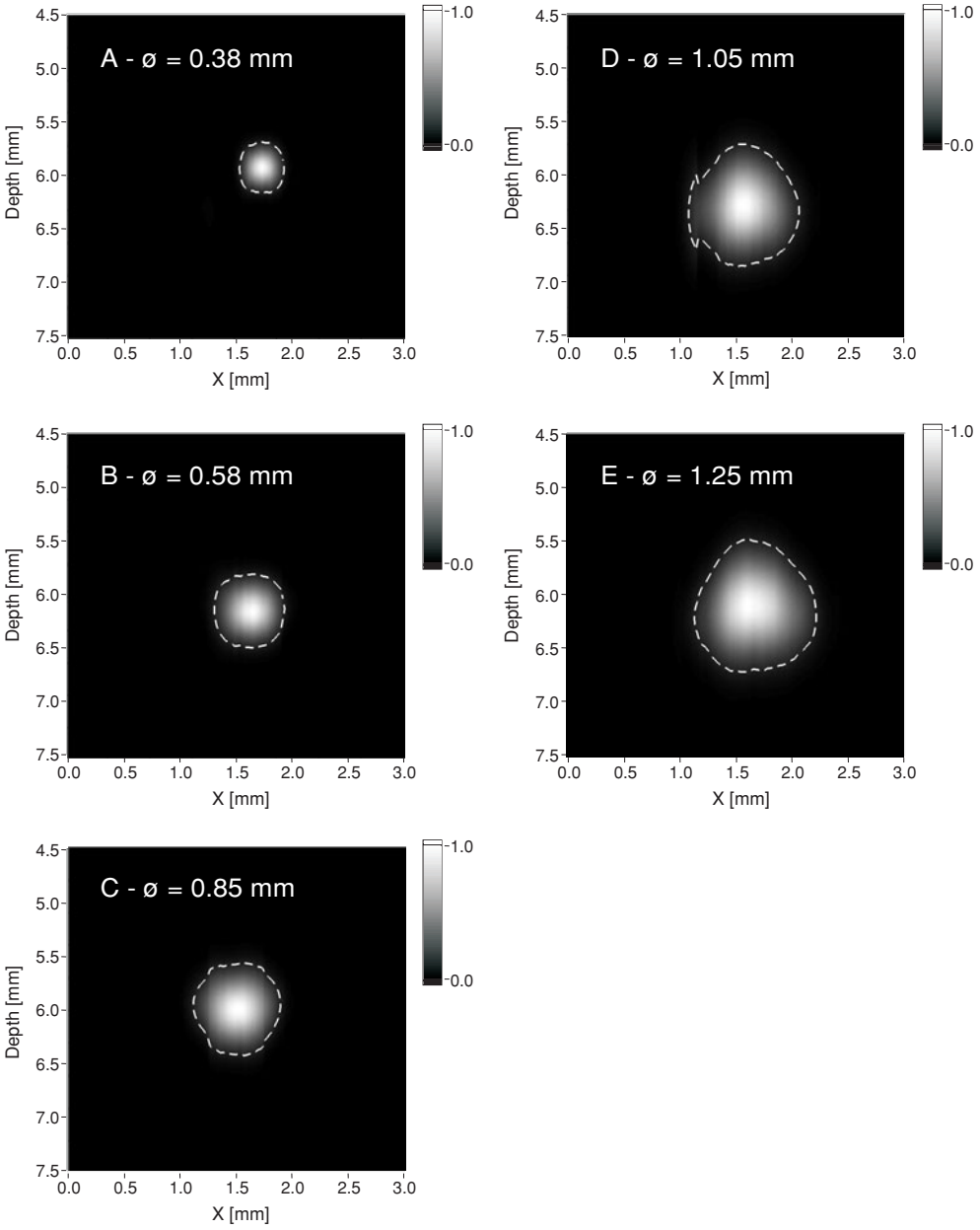

Figure 3. Photoacoustic reconstruction of the cross-section of artificial blood vessels, with five different inner diameters (indicated in the images), filled with flowing human blood, and situated in 10% Intralipid-10%. The diameter of the vessels as estimated with our model is indicated by a dashed contour (e^{-2}); in these images only a subset of the original scan-data is plotted.

(figures 3(A) to (E)). Using the scaling factor $a = 2$, the contours (e^{-2}) corresponding to the estimated diameter of the vessels could be obtained (dashed lines in figures 3(A) to (E)).

From these images, the lateral diameter was estimated which correlated very well with the diameter as measured with a microscope (figure 4). Furthermore, the obtained lateral

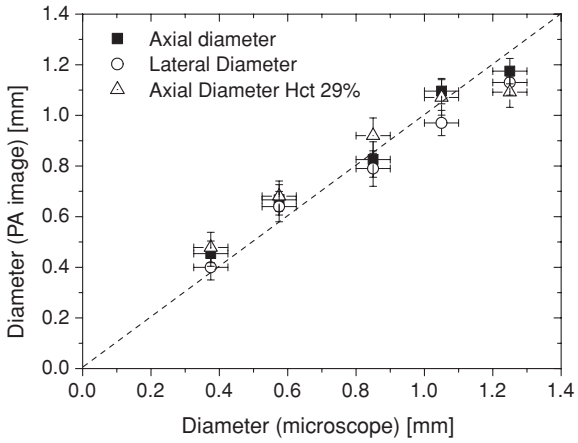

Figure 4. Diameter in axial and lateral direction for whole blood (hematocrit = 49%) together with diameter in axial direction for diluted blood (hematocrit = 29%). The dashed line represents the expected one-to-one relation between the estimated (PA image) and actual (microscope) diameter.

diameters were very close to the measured axial diameter for whole blood (hematocrit 49%) and for diluted blood (hematocrit 29%).

4.2. In vivo experiments

The whole procedure to reconstruct the absorption distribution could also be applied to *in vivo* data. In figure 5(A), the absorption distribution is shown of the auricular artery in the rabbit ear, at the position indicated by line 1 in figure 1. This photoacoustic image shows an elliptic cross-section of the vessel that has an axial diameter of 1.2 mm and a lateral diameter of 1.7 mm.

Similarly, along line 2 (figure 1), the bifurcating vessels could be reconstructed (figure 5(B)). The two vessels are indicated with 1 and 2. To monitor vessel dimensions *in vivo*, the sensor was placed in one steady position above the centre of vessel 1 in figure 5(B), at position $X = 1.5$ mm. The changes in vessel diameter by intermittent upstream vessel occlusion could clearly be monitored (figure 6). In figure 6(A) the photoacoustic time traces during and after occlusion are shown, together with a bipolar photoacoustic signal that was fitted to the measured pressure transients. The vessel diameter was determined from the peak-to-peak time (figure 6(B)) and during occlusion a reproducible decrease in vessel diameter of about 25% from 0.8 mm to 0.6 mm could be observed.

The photoacoustic time trace of a vessel filled with blood has been compared with the time trace of a vessel filled with saline (figure 7(A)). The main bipolar pressure transient disappeared almost completely when the blood was replaced by saline. A bipolar photoacoustic signal (equation (2)) was fitted to the measured pressure transient. The normalized amplitude of the fit has been determined as a function of time (figure 7(B)). During the time that the vessel was flushed with saline the amplitude showed a distinct decrease, whereas it returned to the original value immediately when the flushing with saline was stopped.

5. Discussion

In this paper the use of photoacoustic imaging to reconstruct the absorption distribution was demonstrated. From these distributions the axial and lateral diameters of blood vessels could

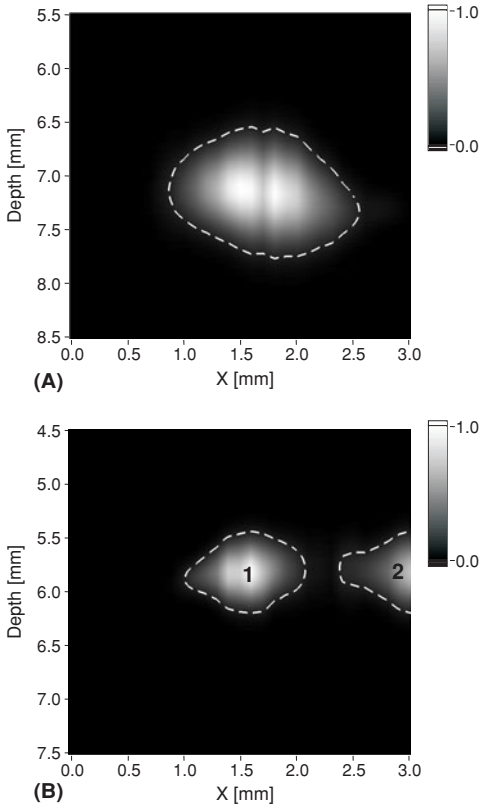

Figure 5. (A) Photoacoustic reconstruction of a vessel in the rabbit ear (line 1, figure 1), only a subset of the original scan-data is plotted. (B) Photoacoustic reconstruction of two vessels close to each other in rabbit ear (line 2, figure 1).

be obtained *in vitro* and *in vivo*. Furthermore, monitoring of changes in the vessel diameter in a rabbit ear was feasible.

5.1. Implications and limitations of our model

The images of the artificial vessels showed that the reconstructed cross-section has a circular shape (figure 3), which means that the lateral and axial diameters of the vessel are equal and that our reconstruction algorithm works adequately.

Fitting the model of equation (5) to the estimated peak-to-peak times yielded that the vessel diameter can be approximated by

$$\tau_{pp} = \sqrt{\left(\frac{\phi}{2c}\right)^2 + \tau_l^2}. \tag{7}$$

This expression is plotted as a dashed line in figure 2. In the case where the diameter of the vessel is much larger than $2c\tau_l$, i.e. much larger than 16.5 μm, the contribution of the laser pulse duration to the peak-to-peak time can be neglected and the diameter can be approximated by $\phi = 2c\tau_{pp}$. Comparing equation (7) with the expression for a spherical Gaussian source (equation (3)) shows that the diameter ϕ of a cylindrical source is equal to four times R_σ, the $1/\sqrt{e}$ radius of the Gaussian source.

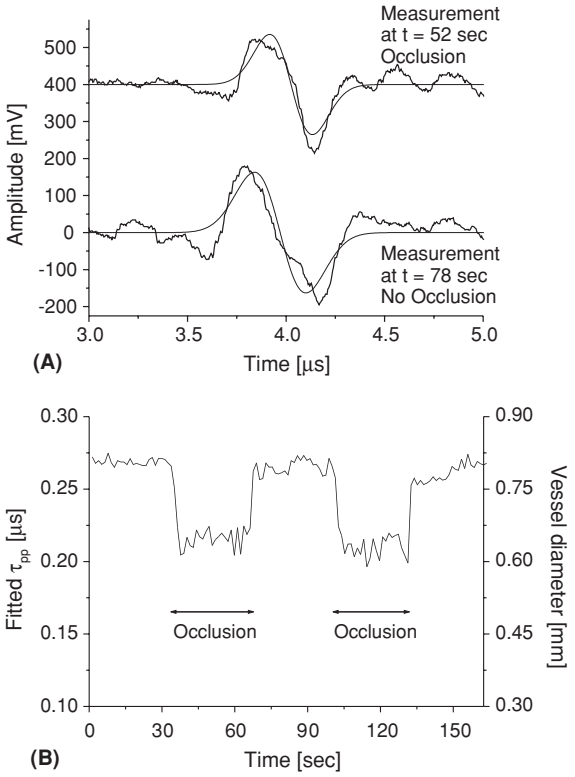

Figure 6. (A) Photoacoustic time traces during (at $t = 52$ s) and after (at $t = 78$ s) occlusion, together with the fitted bipolar signal (time trace during occlusion is shifted over 400 mV). (B) Vessel diameter determined from peak-to-peak time (τ_{pp}) of the fitted bipolar signal traces during monitoring at one steady position above the vessel, while the vessel is repetitively closed (occlusion) and opened.

For the larger diameters, our measurements are limited by the frequency response of the system. The amplifier system of our sensor contains a high pass filter with a cut-off frequency of 800 kHz (−6 dB). This precludes measurements on vessels that generate pressure transients with a main frequency that is below 800 kHz. Therefore, no measurement was performed on vessels larger than 1.2 mm as in that case the bandwidth limit of the amplifier would influence the measured pressure transients.

Next to these technical limitations, also the imaging conditions will limit the feasibility of our approach. In the case of, e.g., large superficial vessels, the vessel will, by its size, shield a part of the light and prevent the light from reaching the side that is most remote from the point of illumination (bottom side of the vessel). In this case only the upper part of the vessel will contribute to the pressure transient. As a result it is expected that the cross-sectional image will flatten at the bottom side and that the peak-to-peak time of the pressure transient will reach a constant value, determined by the penetration depth of the light into the blood vessel. This shielding effect will become less when the depth of the vessel increases as in that case the light becomes more diffuse and the vessel will be illuminated from all sides.

Another limiting situation occurs for large vessels, homogeneously illuminated from all sides, with a diameter much larger than the effective penetration depth of the light into the vessel. In that case only the outer shell of the vessel will contribute to the pressure transient

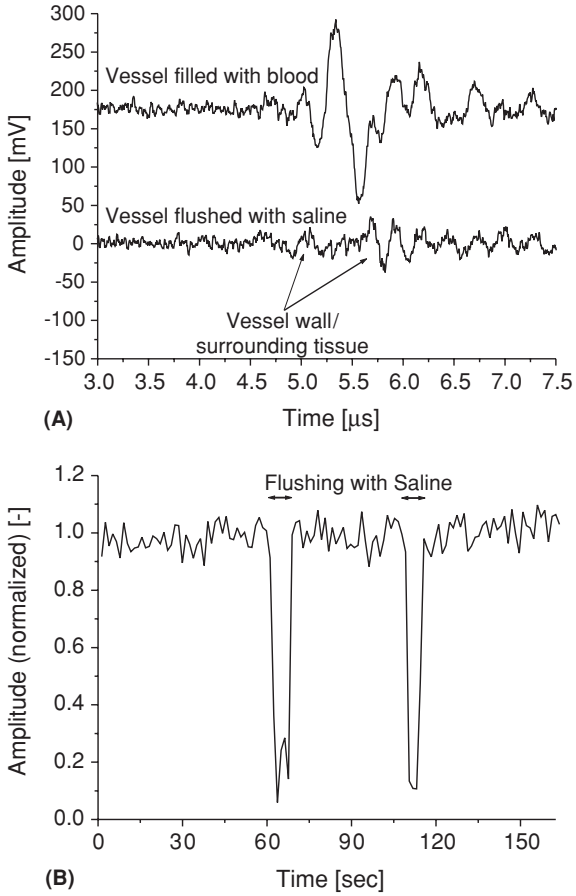

Figure 7. (A) Photoacoustic time trace before flushing with saline (vessel filled with blood) and during flushing with saline; the time trace of vessel filled with blood is shifted over 175 mV. (B) Normalized amplitude of photoacoustic signal during experiment in which blood vessel is flushed with saline.

as the light intensity reaching the inner side of the vessel decreases with increasing depth into the vessel. As is shown by the model of Hoelen and de Mul (1999) the pressure transient in this case consists actually of two pressure transients representing the front and backside of the vessel. From these pressure transients still the vessel diameter can be determined although it will be difficult to determine if these pressure transients originate from one large vessel or from two smaller vessels with a size reflecting the penetration of light into the large vessel.

So it is expected that the peak-to-peak time of the pressure transient will reach a constant value for increasing vessel size. This value will represent the effective photoacoustic source-size that is related to the penetration depth of the light into the blood vessel. As a result the maximum vessel diameter, for which our relation between peak-to-peak time and vessel diameter holds, will be dependent on the optical properties of the blood, i.e. absorption and scattering. This implies that the maximum vessel diameter that can be estimated is dependent on wavelength as well as the oxygen saturation of the blood.

Our results showed a good correspondence between the axial and lateral diameter for whole blood (hematocrit 49%) and the axial diameter for diluted blood (hematocrit 29%).

This indicates that the application of our model is not limited to whole blood only and that it can also be applied in cases where the blood has a lower absorption coefficient.

5.2. In vivo experiments

The resulting photoacoustic images of blood vessels in the rabbit ear demonstrate that the cross-section of these vessels can be visualized. The elliptical cross-section of the vessel in figure 5(A) is caused by scanning obliquely over the vessel (figure 1, line 1).

Next, the vessel diameter was monitored during occlusion and re-opening of the vessel. When the vessel (artery) is closed upstream, its internal pressure decreases, causing the vessel to partly collapse. As the photoacoustic signal contains information about the vessel size, characterized by the peak-to-peak time, a decrease in this peak-to-peak time is expected during occlusion. This action was performed on the vessel marked with 1 in figure 5(B). The diameter of this vessel was 0.8 mm, which is in the range where one is able to estimate the vessel diameter from the peak-to-peak time, as shown in figure 2. During repetitively opening and occluding the vessel a change of 25% in vessel diameter was observed (figure 6(B)). This demonstrates that photoacoustic imaging can be used to monitor the diameter of small superficial vessels.

Finally, the vessel was flushed with saline to investigate the contribution of the vessel wall to the laser-induced pressure transient. From this measurement it appeared that the main contribution to the photoacoustic pressure transient comes from the blood inside the vessel. The time traces in figure 7(A) show a small pressure transient at the positions where the vessel wall is expected. During the flushing with saline, the amplitude showed a distinct decrease (figure 7(B)), whereas it returned to the original value immediately when the flushing with saline is stopped. During flushing, a small signal is still present, which probably is generated by small amounts of blood present in the vessel wall or the surrounding tissue.

Measurement of vessel diameter may have a clinical application in, e.g., determination of distensibility of superficial vessels. Stiffer vessels with decreased distensibility occur in persons with higher levels of cardiovascular risk factors. Therefore, non-invasive measures of distensibility are useful in measuring subclinical vascular changes related to arteriosclerosis (Urbina *et al* 2002). For this application the diameter of the vessel should not be too large as it is expected, as is described above, that in that case only a part of the vessel is contributing to the pressure transient. Furthermore, the accuracy of our method has to be improved to be able to detect sufficiently small changes in vessel diameter.

6. Conclusions

The potential of photoacoustic imaging to determine the size of small blood vessels from the measured pressure transient has been explored for an excitation wavelength of 1064 nm. From the laser-induced pressure transient, the diameter ϕ of superficial blood vessels can be estimated from the peak-to-peak time τ_{pp} and the speed of sound in blood c by the relationship $\phi = 2c\tau_{pp}$. The maximum vessel diameter for which this approximation is valid will be dependent on the effective photoacoustic source size, which is determined by the optical properties of the blood, and thus is dependent on the wavelength and oxygen saturation of the blood. The estimation of the vessel diameter from peak-to-peak time is independent of the type of detector or type of image reconstruction algorithm used, provided that the bandwidth of the detector is sufficient to detect the pressure transient undistorted. This model was successfully applied in monitoring changes in vessel diameter *in vivo* in the ear of a rabbit. Finally, it was

proven that the main contribution to the laser-induced pressure transient is caused by blood inside the vessel and that the vessel wall gives only a minor contribution.

Acknowledgment

This work was supported by the Netherlands Technology Foundation STW (grant TTN4661) and the Netherlands Foundation of Fundamental Research on Matter FOM (grant 00PMT22).

References

Beard P C, Hurrel A M and Mills T N 2000 Characterization of a polymer film optical fiber hydrophone for use in the range 1 to 20 MHz: a comparison with PVDF needle and membrane hydrophones *IEEE Trans. Ultrason. Ferroelectr. Freq. Control* **47** 256–64

Hoelen C G A and de Mul F F M 1999 A new theoretical approach to photoacoustic signal generation *J. Acoust. Soc. Am.* **106** 695–706

Kolkman R G M, Hondebrink E, Steenbergen W and de Mul F F M 2003 *In vivo* photoacoustic imaging of blood vessels using an extreme-narrow aperture sensor *IEEE J. Sel. Top. Quantum Electron* **9** 1–4

Kolkman R G M, Hondebrink E, Steenbergen W, van Leeuwen T G and de Mul F F M 2004 Photoacoustic imaging with a double-ring sensor featuring a narrow aperture *J. Biomed. Opt.* **9** at press

Kruger R A, Kiser W L, Reinecke D R, Kruger G A and Miller K D 2003 Thermoacoustic optical molecular imaging of small animals *Mol. Imag.* **2** 113–23

Niederhauser J J, Frauchiger D, Weber H P and Frenz M 2002 Real-time optoacoustic imaging using a Schlieren transducer *Appl. Phys. Lett.* **81** 571–3

Niederhauser J J, Jaeger M and Frenz M 2003 Comparison of laser-induced and classical ultrasound *Proc. SPIE* **4960** 118–23

Oraevsky A A, Karabutov A A, Solomatin S V, Savateeva E V, Andreev V G, Gatalica Z, Singh H and Fleming R D 2001 Laser optoacoustic imaging of breast cancer in vivo *Proc. SPIE* **4256** 6–15

Paltauf G, Schmidt-Kloiber H, Köstli K P and Frenz M 1999 Optical method for two-dimensional ultrasonic detection *Appl. Phys. Lett.* **75** 1048–50

Payne B P, Venugopalan V, Mikić B B and Nishioka N S 2003 Optoacoustic tomography using time-resolved interferometric detection of surface displacement *J. Biomed. Opt.* **8** 273–80

Sigrist M W and Kneubühl F K 1978 Laser generated stress waves in liquids *J. Acoust. Soc. Am.* **64** 1652–63

Urbina E M, Brinton R, Elkasabany A and Berenson G S 2002 Brachial artery distensibility and relation to cardiovascular risk factors in healthy young adults (the Bogalusa heart study) *Am. J. Cardiol.* **89** 946–51

van Staveren H J, Moes C J M, van Marle J, Prahl S A and van Gemert M J C 1991 Light scattering in Intralipid-10% in the wavelength range of 400–1100 nm *Appl Opt.* **30** 4507–14

Viator J A, Choi B, Ambrose M, Spanier J and Nelson J S 2003 In vivo port-wine stain depth determination with a photoacoustic probe *Appl. Opt.* **42** 3215–24

Wang X D, Pang Y J, Ku G, Stoica G and Wang L V 2003 Three-dimensional laser-induced photoacoustic tomography of mouse brain with the skin and skull intact *Opt. Lett.* **28** 1739–41